A semi-analytical numerical method for modelling the normal wheel–rail contact

Aquib Qazi, Honoré Yin, Michel Sebès, Hugues Chollet, Cédric Pozzolini

Taylor & Francis
Taylor & Francis Group

Vehicle System Dynamics
International Journal of Vehicle Mechanics and Mobility

ISSN: (Print) (Online) Journal homepage: www.tandfonline.com/journals/nvsd20

A semi-analytical numerical method for modelling the normal wheel–rail contact

Aquib Qazi, Honoré Yin, Michel Sebès, Hugues Chollet & Cédric Pozzolini

To cite this article: Aquib Qazi, Honoré Yin, Michel Sebès, Hugues Chollet & Cédric Pozzolini (2022) A semi-analytical numerical method for modelling the normal wheel–rail contact, Vehicle System Dynamics, 60:4, 1322-1340, DOI: 10.1080/00423114.2020.1854319

To link to this article: https://doi.org/10.1080/00423114.2020.1854319

Published online: 01 Dec 2020.

VEHICLE SYSTEM DYNAMICS
2022, VOL. 60, NO. 4, 1322–1340
https://doi.org/10.1080/00423114.2020.1854319

A semi-analytical numerical method for modelling the normal wheel–rail contact

Aquib Qazi [a,b,c], Honoré Yin [b], Michel Sebès [a], Hugues Chollet [a] and Cédric Pozzolini [c]

[a]COSYS-GRETTIA, Univ Gustave Eiffel, IFSTTAR, Marne-la-Vallée, France; [b]Laboratoire Navier, École des Ponts ParisTech, Univ Gustave Eiffel, CNRS, Marne-la-Vallée, France; [c]ESI Group, Paris, France

ABSTRACT

A new semi-analytical boundary element method is proposed for determining the wheel–rail contact zone and the normal stress distribution within it. The potential contact area is discretised using strip elements, employing an iterative algorithm to satisfy the contact constraints. At each iteration, the length of the contact strips is updated using an analytical expression based on Hertz's theory. This simplified formulation provides good approximation of the pressure distribution, and consequently the contact area, in non-elliptic cases. The reduction in the number of system unknowns by using a semi-analytical methodology also enables fast computation speeds, an indispensable requirement in railway dynamics.

ARTICLE HISTORY
Received 17 August 2020
Revised 3 November 2020
Accepted 16 November 2020

KEYWORDS
Wheel–rail contact; Hertz; non-elliptic contact; vehicle dynamics; contact mechanics; boundary element method

1. Introduction

Safety, track fatigue analyses, and maintenance of railway vehicles are only some of the applications that highlight the importance of wheel–rail contact models. The complexity of different operations necessitates very different levels of modelling: a simplified and coarse model may often be sufficient. For hardware-in-the-loop simulations, where the calculations must be carried out in real time over railway tracks which are several kilometres long, very approximate wheel–rail contact models are generally used. Conversely, other applications require more sophisticated models, as in the estimation of wear in urban rail networks, or the assessment of rolling contact fatigue. The shape of the contact area and the stress distribution within it categorise the different normal contact models available in the literature [1–4].

The case of normal contact between two continuous and non-conforming bodies was first treated by Hertz [5], by assuming frictionless contact and each solid body as an elastic half-space. The Hertzian solution is characterised by an elliptical contact patch, with a semi-ellipsoidal normal pressure distribution acting within the contact area. This approach is limited to profiles with constant curvature, and therefore may lead to approximate results in railway applications where the curvature of the profiles changes along the width of the rail section.

CONTACT Aquib Qazi aquib.qazi@univ-eiffel.fr

The use of discrete methods offers a more realistic approximation of the contact conditions in real-life applications. The finite element method (FEM) has already been used in various studies for elasto-plastic stress analyses and creep force characteristics, employing both implicit and explicit approaches [6,7]. Certain recent works have also used Nitsche's method for frictional contact problems, as opposed to the classical penalty methods or mixed methods, which offers good convergence and robustness [8]. Variational methods as the one described by Kalker's complete theory [9] and implemented in the program CONTACT [10], the boundary element method (BEM) like the one presented by Knothe and Le The [11], or the matrix inversion method (MIM) by Johnson [12] also enable a good estimation of the contact properties. The full normal problem has also received much attention for the contact of rough surfaces [13,14]. Despite the advances in computational prowess in recent years, discrete methods continue to struggle in terms of their capability to be used online in vehicle dynamics simulations. A very fine discretisation is usually required with FEM approaches to satisfactorily represent the contact patch boundaries, while classical boundary element methods require iterative techniques over large potential contact grids to verify the stress constraints.

In most multi-body simulation (MBS) codes, a compromise is reached between the level of accuracy that is deemed acceptable and the time it takes to solve the contact problem. Several approximate tangential contact approaches have been developed with the goal of being implemented in MBS software packages, most notably FASTSIM [15]. Other methods such as the Vermeulen–Johnson model [16], the Shen–Hedrick–Elkins model [17], the Book of Tables by Kalker (USETAB) [18], the Polach model [19] and FaStrip [20] are also used, but they remain restricted to elliptical contact patches. Piotrowsky et al. [21] have extended USETAB to be used in non-Hertzian cases, approximating the contact patch by a single double-elliptical contact. Ayasse and Chollet [22] have adapted FASTSIM to be used in the case of strips instead of ellipses, and a similar approach has also been used with FaStrip in [23]. For the normal contact problem, the desire for real time dynamic simulations has given rise to an intermediate level of approximate methods based on the theory of virtual penetration (VP) of the contacting surfaces. These methods include the Linder model [24], the Kik–Piotrowski model [25], the semi-Hertzian model (STRIPES) [22], and the extended Kik–Piotrowski (EKP) model [26] amongst others. The contact area in these approaches is approximated using the area in which the surfaces would interpenetrate geometrically (overlap) if there is no deformation. This overlapping area is bigger than the actual contact patch, and a scaling factor is used to prescribe the virtual penetration such that the interpenetration zone approaches the real contact area. The technique used for determining the scaling parameter is what broadly differentiates these approaches [27]. There exists in parallel another family of models wherein the non-elliptical part of the contact area is approximated using a series of individual ellipses. This so-called multi-Hertzian method, proposed by Pascal and Sauvage [28], is further simplified by Ayasse et al. [29] to an analytical approach. Some of the questions raised regarding these models, when compared against VP methods in [2], have been addressed recently by Pascal [30].

A proposed improvement to these normal contact models is through the introduction of an analytical approximation for the surface deformation in the ANALYN method [31]. Although the results are promising in comparison to other simplified methods, this method remains sensitive to the negative-curvature correction, a characteristic of all point-based contact models based on Hertz' theory. This makes it challenging to implement the method

as a true black-box solution in dynamic vehicle simulation. It is generally noted that this approach gives a good approximation of the contact area when the pressure distribution estimated is also accurate. Using a more thorough approach in the above family of methods, a better approximation of the pressure distribution should lead to better estimation of the contact patch, which forms the basis of the new semi-analytical approach proposed in this article.

A reduced formulation of the contact between two elastic half-spaces is used in the first part together with a Hertzian model to solve the normal contact, following a semi-analytical methodology. The novel method is then validated using the results from STRIPES [22], ANALYN [31], and CONTACT [10] with theoretical as well as wheel–rail profiles. A comparison of the required computational resources is also carried out using different approaches, before the final conclusions.

2. Methodology

2.1. Theoretical background

The problem describing the stress field in a semi-infinite half-space, subjected to a concentrated normal surface force, was studied in detail by Boussinesq [32]. For the half-space consideration to be valid locally, the contact area dimensions must be significantly smaller as compared to the principal radii of the contacting surfaces. This is generally true when considering several common contact scenarios such as the tread contact between wheels and rails. The following assumptions are also made:

- the bodies are elastic, homogeneous and isotropic;
- the contacting surfaces have a continuous profile;
- the normal and tangential problems can be solved sequentially.

One possible solution is using the potential theory of Boussinesq [32], described exhaustively in the book by Johnson [12]. The normal elastic displacement $\bar{u}(x, y)$ is related to the normal pressure distribution $p(x, y)$ by the integral equation [33]

$$\forall (x, y) \in \Sigma, \quad \bar{u}(x, y) = \iint_{\Sigma_c} p(\xi, \eta) T(x, y; \xi, \eta) \, \mathrm{d}\xi \, \mathrm{d}\eta, \tag{1}$$

where Σ is the half-space domain under consideration, Σ_C is the zone of the contact, and T is Boussinesq's influence function defined as

$$\forall (x, y; \xi, \eta) \in \Sigma^2, \quad T(x, y; \xi, \eta) = \frac{1}{\pi E^\star} \frac{1}{\sqrt{(x - \xi)^2 + (y - \eta)^2}}. \tag{2}$$

$E^\star$ is the effective Young's modulus of elasticity for the two contacting bodies Ω_1 and Ω_2 such that

$$\frac{1}{E^\star} = \left(\frac{1 - \nu_1^2}{E_1} + \frac{1 - \nu_2^2}{E_2} \right), \tag{3}$$

where E_1 and E_2 are the modulus of elasticity for the two solids, while ν_1 and ν_2 are the respective Poisson's ratios. With a defined rigid approach δ, the only geometrical input

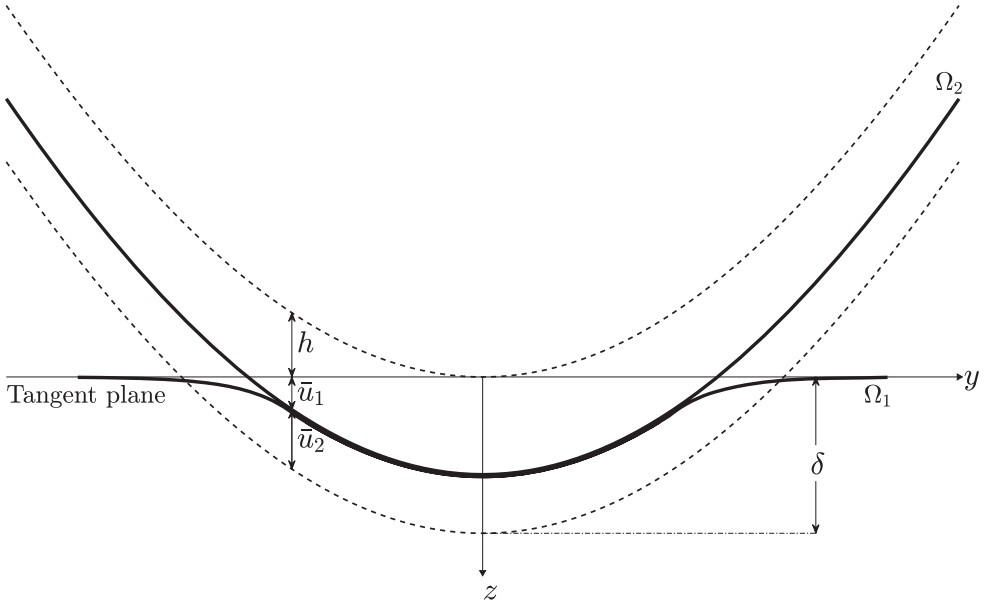

Figure 1. Two elastic bodies in contact.

required to solve the contact problem is the separation between the two undeformed surfaces $h(x, y)$. The normal surface deformation $\bar{u}(x, y) = \bar{u}_1(x, y) + \bar{u}_2(x, y)$ must be evaluated at each point within the contact zone. This contact problem can be summarised in Figure 1. Considering Σ_C as the area of contact, the conditions of Signorini give the cases of separation and of contact as:

$$\forall (x, y) \notin \Sigma_C, \quad \delta - \bar{u}(x, y) - h(x, y) < 0 \text{ and } p(x, y) = 0, \tag{4}$$

$$\forall (x, y) \in \Sigma_C, \quad \delta - \bar{u}(x, y) - h(x, y) = 0 \text{ and } p(x, y) > 0. \tag{5}$$

The boundary conditions defined in Equations (4) and (5) ensure that the normal pressure can only act within the contact zone, vanishing at the boundary of the contact area. The two bodies are also prevented from interpenetrating. The discretised form of the variational inequality eventually gives rise to a linear complementarity problem (LCP). If the rigid approach δ is given, the problem to be solved can be completely described by Equations (1) and (5). If the total resultant force N is known in advance, the following equilibrium condition is added:

$$\forall (x, y) \in \Sigma_C, \quad N = \iint_{\Sigma_c} p(\xi, \eta)\, \mathrm{d}\xi\, \mathrm{d}\eta. \tag{6}$$

2.2. Towards a reduced approach

The classical direct method to solve the contact problem is the matrix inversion method (MIM) found in [12]. The potential contact area in the boundary element problem is overestimated in both the lateral as well as the rolling directions, and divided into a rectangular

grid, wherein the contact constraints of Equations (4) and (5) are evaluated. The elements in which the pressure distribution has negative values are discarded, and the procedure is repeated until all the remaining elements satisfy the boundary conditions. The elastic deformation is thus calculated at each iteration for each element within the potential contact area, resulting in a sizeable expenditure of computational resources. The drawback of using such an approach is clear, as the direct method does not scale to large-sized problems. Certain studies also use iterative techniques such as Gauss-Seidel, which however remains restricted to relatively small contact grids. Most recent works use either a conjugate gradient (CG) algorithm or a multi-grid (MG) strategy, combined with fast algorithms such as multi-level summation technique (MLMS) or fast Fourier transform (FFT) for equation solving [13,14]. The spirit of these approaches remains the same: using different numerical techniques for a faster solution of the complete LCP. In the proposed new approach, the pressure distribution is additionally assumed to be symmetric and elliptic about the $x = 0$ plane and the potential area of contact is discretised only in the lateral y direction. A similar strategy for discretisation is also used by Reusner for the treatment of roller bearings in [34], and by Knothe and Le The for more arbitrary elastic bodies in [11]. Along with the normal stress distribution acting on each strip, Reusner considers the lengths of the contact patch strips as supplementary unknowns, while Knothe and Le The attempt to further reduce the computational complexity by showing that the strip lengths in neighbouring elements should vary almost proportionally with the variations in the load or the deflection. The novel approach in the present paper is to instead consider the contact patch boundaries as a quasi-known quantity dependent on the form of the normal stress distribution. The potential contact area is first divided into thin strips with the larger dimension in the rolling direction, as shown in Figure 2, from where the name MIM-1D is chosen for the new method. The unknown in this case reduces to the maximum pressure values p_{0_i} at the centre of each strip i. At each iteration, the half-length of the contact strip a_i in the rolling direction is then computed as a function of the maximum pressure distribution p_{0_i}, using an approximate analytical formulation based on Hertz' theory.

2.3. Discrete problem

The half-length and the half-width of each strip element are given as a_i and b_i, respectively. The pressure distribution over each strip is assumed to be semi-elliptical in the x direction, and constant in the y direction. Thus, the expression for the pressure distribution over each strip may be written as

$$p(x, y_i) = p_{0_i}\sqrt{1 - \left(\frac{x}{a_i}\right)^2}, \tag{7}$$

where p_{0_i} is the maximum pressure at the centre (x_i, y_i) of the strip i. The deformation and the separation at the centre are denoted as u_i and h_i, respectively. Equations (1) and (5) in discrete form are:

$$\forall i \in [1, n], \quad u_i = \sum_{j=1}^{n} C_{ij} p_{0_j}, \tag{8}$$

$$\forall i \in [1, n] \ni (x_i, y_i) \in \Sigma_C, \quad \delta - u_i - h_i = 0 \text{ and } p_{0_i} > 0, \tag{9}$$

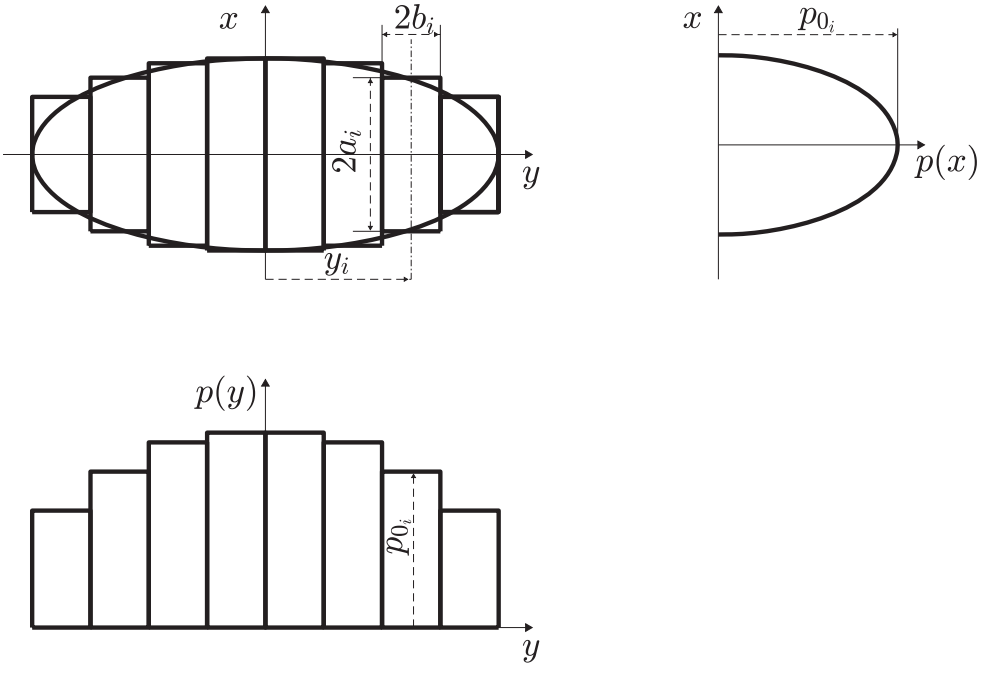

Figure 2. Contact area Σ_C divided into strips, and the normal pressure distribution [11].

where n denotes the total number of elements in the potential contact area. The terms C_{ij} from Equation (8) are called the coefficients of influence, and are defined as

$$C_{ij} = \frac{2}{\pi E^{\star}} \int_{y_j - b_j}^{y_j + b_j} \int_{0}^{a_j} \frac{\sqrt{1 - (\frac{\xi}{a_j})^2}}{\sqrt{(x_i - \xi)^2 + (y_i - \eta)^2}} \, \mathrm{d}\xi \, \mathrm{d}\eta. \tag{10}$$

The expression for C_{ij} describes the influence of normal stress distribution in the jth element to induce elastic displacement in the ith element. In the previous work by Reusner [34], the influence factors are expressed in the form of complete elliptic integrals. Knothe and Le The [11] determine these factors using numerical integration, however no further details have been provided. In MIM-1D, the C_{ij} terms are also evaluated numerically. The x_i terms are ignored as they always remain zero. Equation (10) is written as:

$$C_{ij} = \frac{2}{\pi E^{\star}} \left[\int_{y_j - b_j}^{y_j + b_j} \int_{0}^{a_j} \frac{\sqrt{1 - (\frac{\xi}{a_j})^2} - 1}{\sqrt{\xi^2 + (y_i - \eta)^2}} \, \mathrm{d}\xi \, \mathrm{d}\eta + \int_{y_j - b_j}^{y_j + b_j} \int_{0}^{a_j} \frac{\mathrm{d}\xi \, \mathrm{d}\eta}{\sqrt{\xi^2 + (y_i - \eta)^2}} \right]. \tag{11}$$

The first integral is regular and can be evaluated numerically using Gaussian quadrature. A higher number of integration points may be chosen closer to the diagonal terms. The second integral is singular when the denominator approaches zero. This expression represents the case of uniform normal pressure acting on a rectangular area of $2a_i \times 2b_i$, and an

analytical solution of this problem has been presented in detail by Love [12,35]. We have

$$2\int_{y_j-b_j}^{y_j+b_j}\int_{0}^{a_j}\frac{\mathrm{d}\xi\,\mathrm{d}\eta}{\sqrt{\xi^2+(y_i-\eta)^2}} = (y+b_j)\log\left[\frac{a_j+\sqrt{(y+b_j)^2+a_j^2}}{-a_j+\sqrt{(y+b_j)^2+a_j^2}}\right] + (y-b_j)\log\left[\frac{-a_j+\sqrt{(y-b_j)^2+a_j^2}}{a_j+\sqrt{(y-b_j)^2+a_j^2}}\right] + 2a_j\log\left[\frac{(y+b_j)+\sqrt{(y+b_j)^2+a_j^2}}{(y-b_j)+\sqrt{(y-b_j)^2+a_j^2}}\right], \tag{12}$$

where

$$y = y_i - y_j.$$

An additional advantage of treating the original integral expression in such a manner is the introduction of an analytical solution into the numerical results. This may consequently reduce the integration error linked to the quadrature method. It also permits the use of lesser number of integration points, and consequently faster calculation times. Equation (8) in matrix form is written as

$$\mathbf{u} = \mathbf{C}\mathbf{p}, \tag{13}$$

where the vectors $\mathbf{p}$ and $\mathbf{u}$ are given as $\{p_{0_1},\ldots,p_{0_n}\}^{\mathrm{T}}$ and $\{\delta-h_1,\ldots,\delta-h_n\}^{\mathrm{T}}$, respectively. The matrix of influence coefficients $\mathbf{C}$ is

$$\mathbf{C} = \begin{bmatrix} C_{11} & \ldots & C_{1n} \\ \vdots & \ddots & \vdots \\ C_{n1} & \ldots & C_{nn} \end{bmatrix}. \tag{14}$$

This is the method of resolution generally followed in the case where the rigid approach δ is known in advance. Unlike in the classical method, $\mathbf{C}$ needs to be evaluated at the beginning of each iteration as the size of the elements in the x direction does not remain the same.

In the case where the normal force is prescribed instead of rigid body approach δ, the normal contact problem is solved with an additional iteration for δ. The resultant force at the end of each iteration is calculated using Equation (6):

$$N = \pi\sum_{i=1}^{n}(a_i b_i)p_{0_i}. \tag{15}$$

The initial value of δ can be taken as the Hertzian rigid body approach. The subsequent values of δ may be evaluated using a dichotomy or an iterative scheme based on Hertz' relations [11]:

$$\delta^{(m+1)} = \delta^{(m)}\left[\frac{N}{\tilde{N}^{(m)}}\right]^{2/3}, \tag{16}$$

where $\tilde{N}^{(m)}$ represents the resultant normal force at the end of mth iteration.

For numerical simulations, it is also possible to modify Equation (13) using the normal force over each strip N_i (see Appendix 1).

2.4. Estimation of the contact patch half-length

The half-length of the contact patch a_i is approximated using the equations that apply in Hertzian cases. a_i is updated at each iteration to define the new potential contact zone, which is then used to construct the matrix **C**. The equation for the Hertzian contact ellipse is

$$\left(\frac{x}{a_0}\right)^2 + \left(\frac{y}{b_0}\right)^2 = 1, \tag{17}$$

where a_0 and b_0 are the semi-axes of the ellipse [36], given by:

$$a_0 = m\left[\frac{3}{2}N\frac{1}{2E^\star}\frac{1}{(A+B)}\right]^{1/3}, \tag{18}$$

$$b_0 = n\left[\frac{3}{2}N\frac{1}{2E^\star}\frac{1}{(A+B)}\right]^{1/3}. \tag{19}$$

Here, A and B are the relative curvatures in the longitudinal and lateral directions, respectively, while m and n are the non-dimensional Hertzian coefficients assessed using the curvatures (see Appendix in [22], or [36]). The normal pressure distribution $p(x, y)$ over the contact area is semi-ellipsoidal, and given by

$$p(x,y) = p_{0_H}\sqrt{1 - \left(\frac{x}{a_0}\right)^2 - \left(\frac{y}{b_0}\right)^2}, \tag{20}$$

with the maximum normal pressure at the centre of ellipse,

$$p_{0_H} = \frac{3}{2}\frac{N}{\pi a_0 b_0}. \tag{21}$$

Equation (17) over each strip can be written as

$$\left(\frac{a_i}{a_0}\right)^2 + \left(\frac{y}{b_0}\right)^2 = 1. \tag{22}$$

Combining Equations (20) and (22), the normal pressure distribution in the longitudinal x direction for the ith strip is

$$p(x,y_i) = p_{0_H}\frac{a_i}{a_0}\sqrt{1 - \left(\frac{x}{a_i}\right)^2}. \tag{23}$$

Comparing Equations (7) and (23), it is possible to deduce

$$p_{0_i} = p_{0_H}\frac{a_i}{a_0} = \frac{3}{2}\frac{N}{\pi a_0 b_0}\frac{a_i}{a_0}. \tag{24}$$

Using the expressions for the semi-axes a_0 and b_0 defined previously, the contact patch half-length can be found using

$$a_i = \frac{\pi}{2E^*}\frac{m^2 n}{A+B}p_{0_i}. \tag{25}$$

This Hertzian expression for the contact patch boundary depends on the geometric properties of the profiles in contact, and the normal pressure at the centre of the strip under consideration. In non-elliptic cases, the curvatures and the Hertzian coefficients are replaced by their local values. Thus,

$$\tilde{a}_i = \frac{\pi}{2E^*}\frac{m_i^2 n_i}{A_i+B_i}p_{0_i}. \tag{26}$$

The same expression for the half-length can also be obtained using the theory of ANALYN (see Appendix 2). Hertz' solution remains valid only for positive values of B_i. If the lateral curvature is negative at a given point, a correction must be carried out. Moreover, if the curvature is discontinuous, a smoothing is also applied. This correction and smoothing is done using the procedure described in [22].

2.5. Iterative resolution

Equation (26) is incorporated into the iterative algorithm presented in Figure 3 to solve the contact problem described by Equation (13). In the presented test cases, the potential contact area is taken as the interpenetration zone using the Hertzian rigid body approach, as this is sufficiently large to enclose the actual contact area. The choice of this potential contact zone is not found to have a significant impact on the convergence of the proposed algorithm. When the problem is specified with only a given penetration, the interpenetration area is the optimal choice. In order to speed up the computation, the matrix of influence coefficients $\mathbf{C}$ is constructed only using the elements i where the separation h_i is less than a predefined maximum value $h_{\max}$. When the resultant normal force N is known, the same algorithm is repeated for each value of $\delta^{(m)}$, evaluated using Equation (16). The total normal force at the mth iteration $\tilde{N}^{(m)}$ is computed using Equation (15). The algorithm in this case converges when a user defined tolerance value $\epsilon = |\tilde{N}^{(m)} - N|$ is attained.

3. Results and discussion

The proposed new approach MIM-1D is implemented as a Matlab function. The approximate surface deformation method ANALYN [31], and the VP method STRIPES [22] are also programmed using Matlab. The results from the commercial version of the program CONTACT (v20.1) [10] are used as the reference. It should be noted that the ANALYN results are sensitive to the method used for the negative-curvature correction. In the original publication, the negative lateral curvature values are replaced using a fifth-degree polynomial. However, this correction strategy has not been explained in further detail, and here this is done heuristically to obtain results as close as possible to the ones presented in [31].

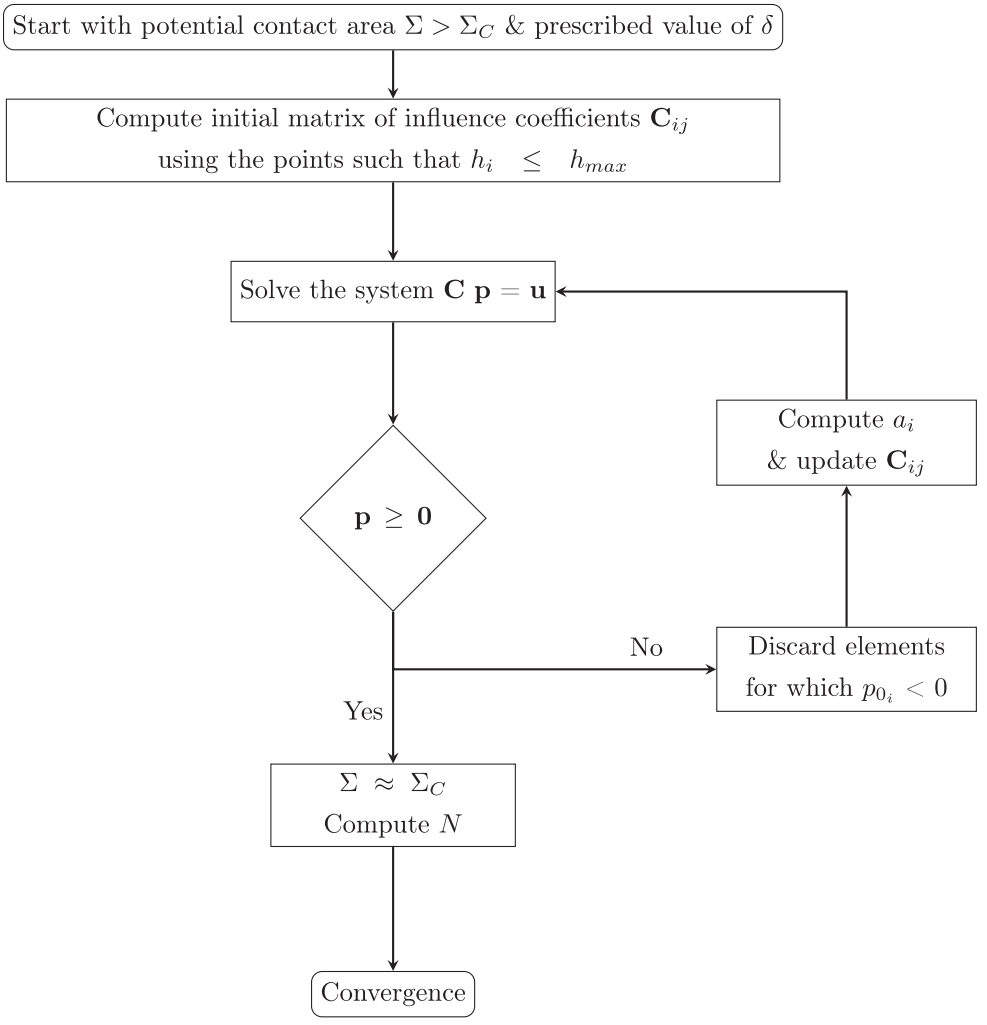

Figure 3. MIM-1D algorithm with a given rigid body approach δ.

3.1. Theoretical profiles

3.1.1. Hertzian

To validate the new approach, a Hertzian case is considered with the contact between a sphere ($R = 40$ mm) and a flat surface. The separation curve between the two surfaces is shown in Figure 4(a). Both bodies are made of steel, with $\nu = 0.3$ and $E = 208$ GPa. The rigid approach between the two bodies is taken as 1 mm.

The contact patches obtained using different approaches and the maximum pressure distribution $p_0(y)$ are shown in Figure 5. All the methods can be observed to be in good agreement with each other. The relative error in the contact area for MIM-1D is found to be within 1% of Hertz's analytical solution, which can be attributed to the accuracy of numerical procedure used.

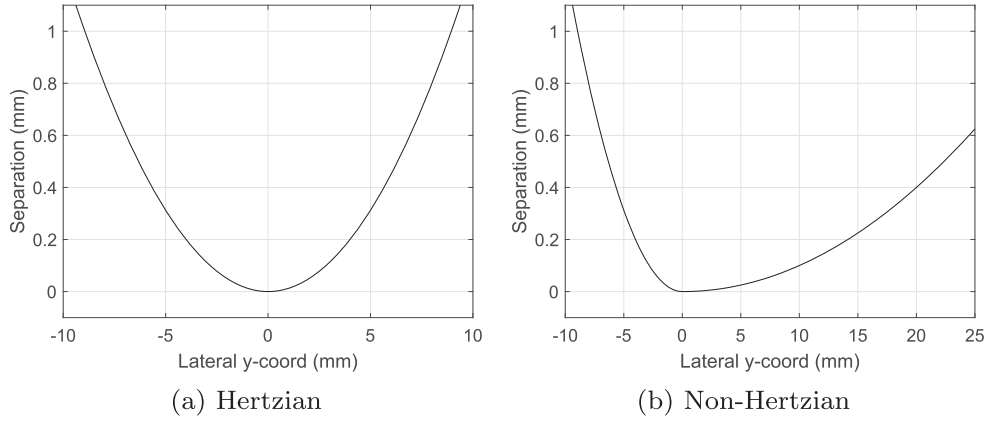

Figure 4. Separation profiles of the two contacting surfaces. (a) Hertzian, (b) non-Hertzian.

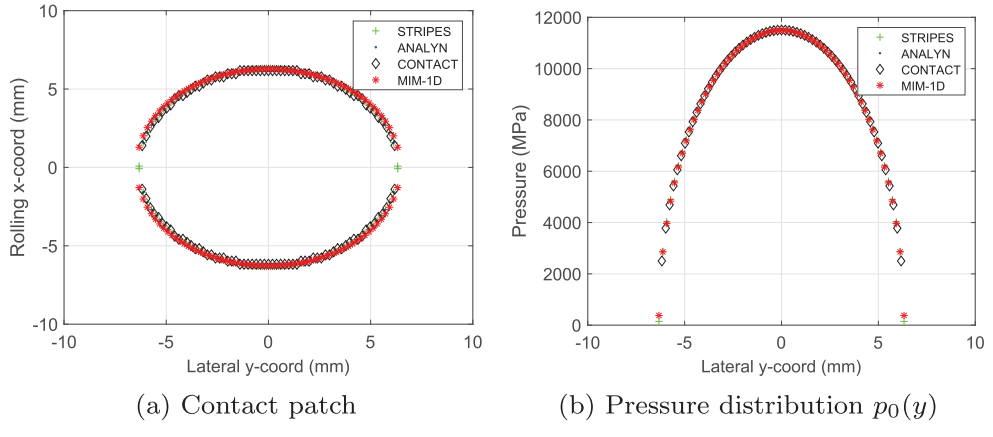

Figure 5. Results for a Hertzian profile using existing methods and MIM-1D. (a) Contact patch. (b) Pressure distribution $p_0(y)$.

3.1.2. Non-Hertzian

The contact between a flat surface, and a body of revolution (rolling radius $R_n = 400\,\text{mm}$) with a non-Hertzian theoretical profile developed using two different radii $R_1 = 40\,\text{mm}$ and $R_2 = 500\,\text{mm}$ on either side of the point of first contact is considered next. The separation curve between the two surfaces is shown in Figure 4(b). The material properties are the same as in the Hertzian case, with the bodies pushed 1 mm towards each other.

The results for the contact area and the maximum pressure distribution are presented in Figure 6. From Figure 6(a), MIM-1D and ANALYN correspond reasonably well with the reference results from CONTACT. The relative error in the contact area for MIM-1D is within 1% of the reference results. STRIPES notably underestimates the width of the contact patch: this is expected, as neglecting the surface deformation should lead to a smaller contact zone. Although the pressure distribution curve for ANALYN in Figure 6(b) follows the same trend as that of the reference, the peak of the pressure curve remains significantly higher. The results using MIM-1D can be observed to be in a better agreement

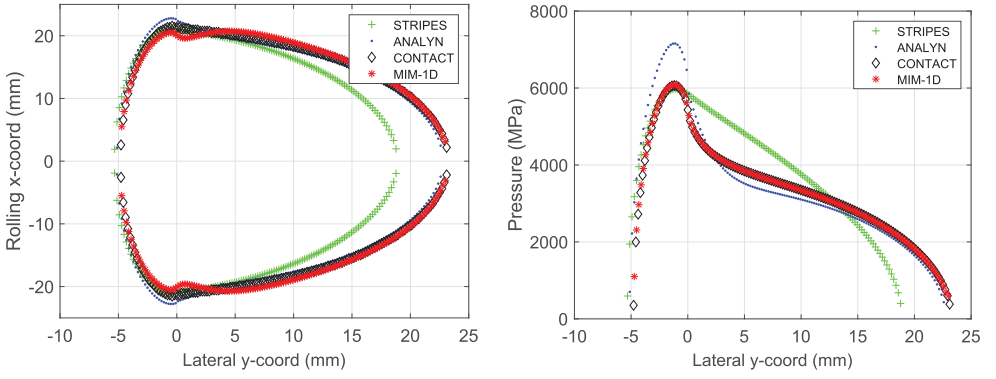

(a) Contact patch (b) Pressure distribution $p_0(y)$

Figure 6. Results for a non-Hertzian profile using existing methods and MIM-1D. (a) Contact patch. (b) Pressure distribution $p_0(y)$.

with the reference method. A characteristic bottleneck region in the contact shape may be observed at around $y = 0$ mm. This can be attributed to Equation (26), which is used to estimate the contact patch length. Even though the stress distribution is relatively continuous over the entire contact zone, the $\tilde{a}_i$ expression is essentially Hertzian. The terms m_i and n_i depend on the procedure used to compute the longitudinal and lateral curvatures A and B, respectively, as well as the negative curvature correction strategy. In the cases where the profile changes abruptly (e.g. $R_1 = 40$ mm to $R_2 = 500$ mm at $y = 0$ mm in Figure 4(b)), the discontinuity in curvatures might introduce a visible discontinuity in the contact area as well. These discontinuities may ultimately be treated in the pre-processing by using a more suitably adapted curvature smoothing process. However, these do not seem to be too significant in the case of wheel–rail contact, where the change in profiles is more gradual and not restricted to a sole point as in the considered theoretical cases.

Simulations are carried out using different potential contact zones to check the influence of this input parameter on the convergence of the proposed algorithm. The resultant normal forces are taken as 963 and 2645 kN (corresponding to $\delta = 1$ mm) for the Hertzian and the non-Hertzian profiles, respectively. These results are presented in Figure 7. The outer loop iterations denote the number of iterations on the value of the applied rigid body approach $\delta^{(m)}$ using Equation (16) to obtain the required resultant normal force. On the other hand, the inner loop iterations represent the average number of iterations required for the convergence of the algorithm presented in Figure 3 for each value of $\delta^{(m)}$. The choice of the potential contact zone visibly does not have a significant impact on the convergence.

3.2. Wheel–rail contact

The case of wheel–rail contact is presented using the standard wheel profile S1002 over the rail profile UIC60, with an inclination of 1:40. The material for both the wheel and the rail is steel. The resultant normal contact force is taken as 78,500 N. The results are presented for various positions of the wheel, displaced from its centre position over the rail, denoted by Δy. The sign convention is taken the same as in [31], where a positive Δy signifies the movement of the contact point towards the wheel flange. The discretisation

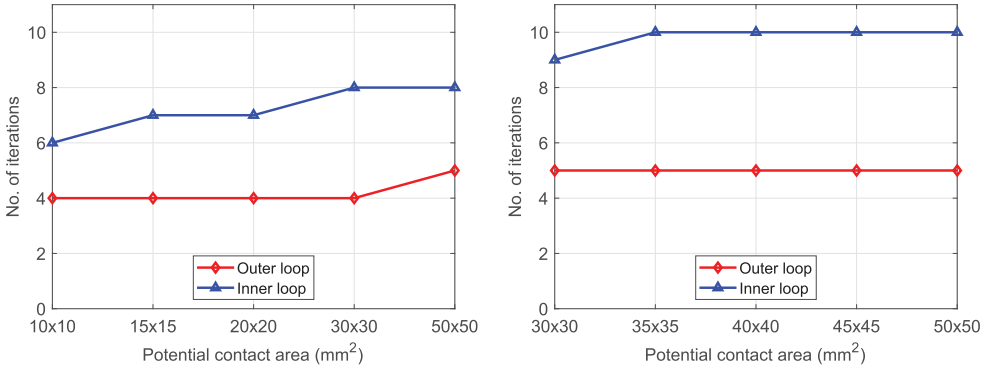

(a) Hertzian (b) Non-Hertzian

Figure 7. Convergence of the proposed algorithm for different potential contact areas. (a) Hertzian, (b) non-Hertzian.

size is taken as approximately 0.2 mm for all the tested cases, which can be considered as a fine discretisation for wheel–rail contact applications.

The test cases are chosen to remain in the tread region with low contact angles, where the half-space assumption is not violated. From Figure 8, the MIM-1D results match closely with the reference CONTACT results in all the presented cases. This is highlighted more prominently in the maximum pressure distribution over the contact patch length. It can also be remarked that MIM-1D manages to accurately capture the characteristic slight variations in the pressure distribution, such as those presented in the tail end of the case $\Delta y = -1$, a trait missing in the other simplified methods. ANALYN remains more precise compared to the VP methods, as neglecting the surface deformation in STRIPES again leads to an underestimated contact zone. The negative curvature compensation procedure used in STRIPES may have an effect as well [37]. This sensibility of STRIPES related to the processing of the curvature is also found to be true in the case of ANALYN, with some fine tuning required to obtain the desired results. A correction strategy dependent on the applied contact force and the separation may possibly improve the results [31]. Figure 9 presents the relative comparison of the contact area for a range of Δy values to the CONTACT results, emphasising the improvement using the new method as compared to existing fast approaches.

3.3. Computational cost

To make a representative comparison of the computational cost, MIM-1D is tested for different mesh sizes using a Hertzian profile. This comparison is done against the other presented methods, i.e. STRIPES [22], ANALYN [31], and CONTACT [10]. The computations are carried out using a 64 bits 2.70 GHz Intel processor. Only the time for the normal contact problem is considered. The CPU time for CONTACT is taken directly from the generated output file, while the other methods are measured using the elapsed CPU time averaged over a finite number of runs. These results are tabulated in Table 1. STRIPES and ANALYN report similar and the fastest CPU times, which is expected as both methods are innately analytical. The latest version of CONTACT, implemented in Fortran, uses a

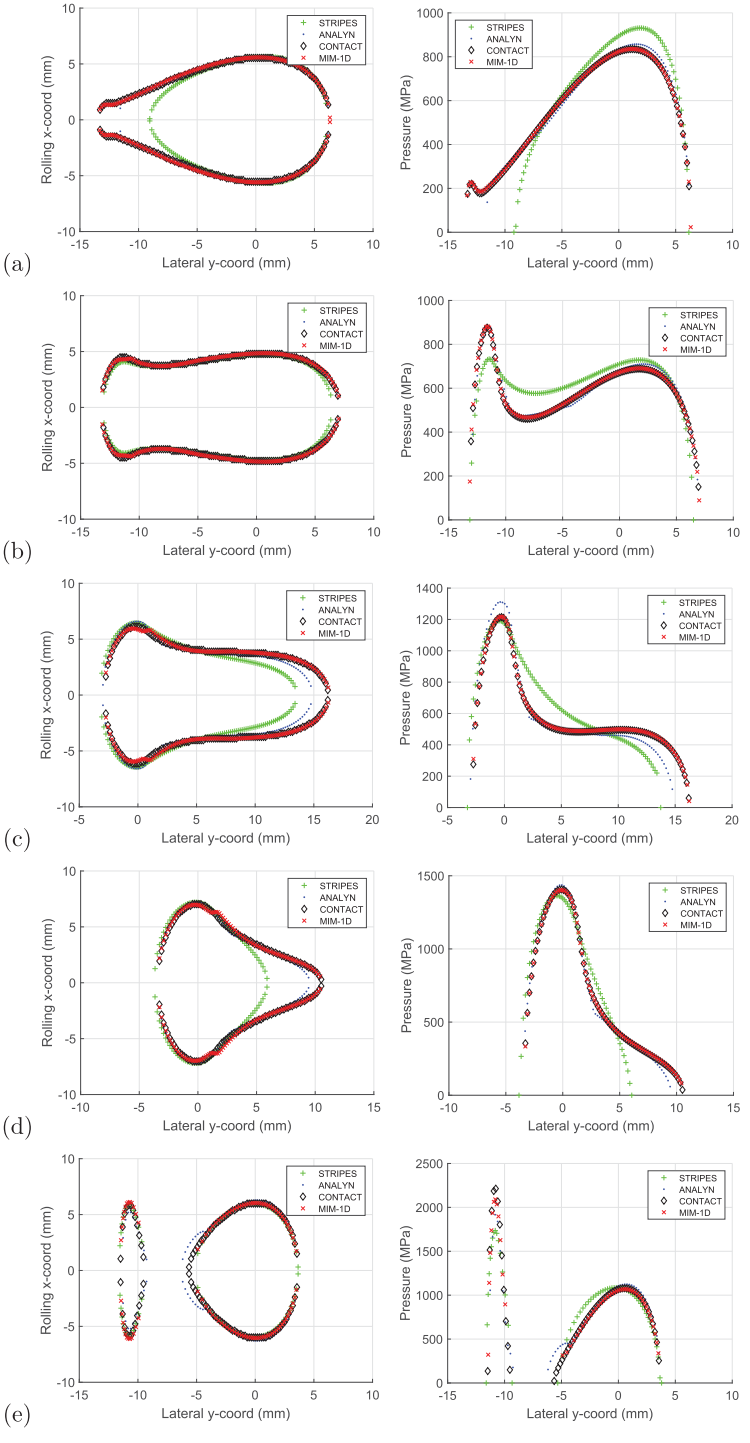

Figure 8. Contact patch (left), and the maximum pressure distribution $p_0(y)$ (right) for wheel–rail contact cases (from top to bottom): (a) $\Delta y = -1$ mm, (b) $\Delta y = 0$ mm, (c) $\Delta y = 1$ mm, (d) $\Delta y = 2$ mm, and (e) $\Delta y = 5$ mm.

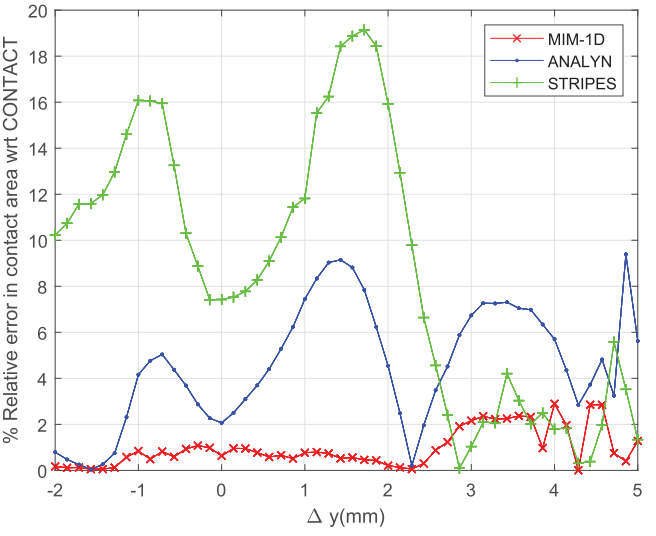

Figure 9. Comparison of the relative error in the contact area with reference results from CONTACT.

Table 1. Comparison of CPU time with existing approaches.

		Time (s)			
Mesh size	n^a	STRIPES	ANALYN	CONTACT	MIM-1D
0.2 mm	100	1.5E−5	6.2E−5	< 0.1	2.0E−3
0.08 mm	250	3.1E−5	9.4E−5	0.2	2.9E−2
0.04 mm	500	9.3E−5	1.3E−4	1.3	9.2E−2

[a]The total number of elements for CONTACT is $n \times n$.

bound-constrained conjugate gradient (BCCG) method with a FFT pre-conditioner which permits reasonably quick solutions even with a very fine discretisation [14]. The MIM-1D implementation here simply employs Matlab's inbuilt solver yet permits a gain in runtime compared to CONTACT, in no small part due to the reduced semi-analytical formulation of the method. Re-evaluating the matrix of influence coefficients at each iteration means that about two-thirds of the CPU time can be spent on the Gaussian quadrature. This may be an interesting guide for future developments, wherein accuracy can be traded for faster computation speeds.

4. Conclusion

A simplified boundary element formulation is presented in this paper and tested against two existing approximate methods, and a complete numerical method used as the reference. In essence, this approach further develops the strip discretisation strategy [11,34] by using a semi-analytical methodology to determine the contact patch dimension in the rolling direction. The novel method, implemented in the algorithm MIM-1D, provides a precise approach comparable to more rigorous complete methods such as CONTACT, with lesser computing effort. The results from the theoretical and wheel–rail test cases presented allow the following conclusions to be drawn:

- The proposed approach MIM-1D enables an improved approximation of the pressure distribution and the contact area as compared to the other existing VP [22] and approximate surface deformation [31] methods.
- Comparison with a complete numerical method for wheel–rail contact shows close agreement, with the relative error in the contact area as compared to the reference results being less than 3% in all the tested cases using theoretical and wheel–rail profiles.
- From Figure 8, the normal stress distribution obtained using MIM-1D for the different test cases can be observed to be in better agreement with the fully detailed method. The peaks of the maximum pressure curve are also noted to conform well with the reference results. This may be seen as a significant advantage in the calculation of wear, that requires the contact stresses instead of the total normal forces.
- The reduction in the number of system unknowns as compared to CONTACT due to a semi-analytical approach provides on an average, a 10-fold speed up with the current Matlab implementation. This should improve further by using a programming language closer to machine language such as Fortran.

It is important to keep in context that the latest versions of CONTACT incorporate advanced numerical techniques to enable faster solving of the normal contact problem [14]. Using similar numerical optimisation strategies should permit further improvement in the performance of MIM-1D, and these will be tested in future developments. Any simplified method of course brings its own set of drawbacks. Limitations with respect to the generality of contact problems, especially when using rough profiles, are the most obvious. Considering the pressure distribution to be symmetric about the $x = 0$ plane also brings restrictions on taking into account the effect of the yaw angle. The bottleneck regions observed in certain cases, related to the abruptly changing curvatures, may demand supplemental inspections. Further developments must also be implemented in order to accurately treat the flange contact, where the contact angle varies significantly in a small zone, thus violating the half-space assumption. These improvements are currently under study, within the context of the implementation of MIM-1D in the MBS code VOCO (VOitures en COurbe). The eventual implementation should account for the coupling with the tangential contact problem, while taking the effect of friction into account. The new approach does not replace any of the previous ones but adds a new method in the spectrum of fast versus detailed methods. With proper optimisation, solving the classical normal contact problem using only strip elements should enable MIM-1D to be used as a good reference for other coarse models commonly employed in dynamic vehicle simulations.

Disclosure statement

No potential conflict of interest was reported by the author(s).

Funding

The authors would like to thank Association Nationale de la Recherche et de la Technologie (ANRT), and ESI Group for their financial support under the CIFRE [Grant No. 2017/1097].

ORCID

Aquib Qazi http://orcid.org/0000-0002-4636-0103

References

[1] Kalker JJ. Survey of wheel–rail rolling contact theory. Veh Syst Dyn. 1979;8(4):317–358.
[2] Piotrowski J, Chollet H. Wheel–rail contact models for vehicle system dynamics including multi-point contact. Veh Syst Dyn. 2005;43(6–7):455–483.
[3] Knothe K. History of wheel/rail contact mechanics: from Redtenbacher to Kalker. Veh Syst Dyn. 2008;46(1–2):9–26.
[4] Meymand SZ, Keylin A, Ahmadian M. A survey of wheel–rail contact models for rail vehicles. Veh Syst Dyn. 2016;54(3):386–428.
[5] Hertz H. Über die Berührung fester elastischer Körper. J Angew Math. 1882;92:156–171.
[6] Zhao X, Li Z. The solution of frictional wheel–rail rolling contact with a 3d transient finite element model: validation and error analysis. Wear. 2011;271(1):444–452. Proceedings of the 8th International Conference on Contact Mechanics and Wear of Rail / Wheel Systems, Florence, 2009.
[7] Toumi M, Chollet H, Yin H. Finite element analysis of the frictional wheel–rail rolling contact using explicit and implicit methods. Wear. 2016;366–367:157–166.
[8] Chouly F, Fabre M, Hild P, et al. An overview of recent results on Nitsche's method for contact problems. In: Bordas SPA, Burman E, Larson MG, et al., editors. Geometrically unfitted finite element methods and applications. Cham: Springer International Publishing; 2017. p. 93–141.
[9] Kalker JJ. Rolling contact phenomena: linear elasticity. In: Jacobson B, Kalker JJ, editors. Rolling contact phenomena. Vienna: Springer Vienna; 2000. p. 1–84.
[10] Vollebregt E. User guide for CONTACT, rolling and sliding contact with friction. Technical report 20-01, version 'v20.2'. Vtech CMCC; 2020.
[11] Knothe K, Le The H. A contribution to the calculation of the contact stress distribution between two elastic bodies of revolution with non-elliptical contact area. Comput Struct. 1984;18(6):1025–1033.
[12] Johnson KL. Contact mechanics. Cambridge: Cambridge University Press; 1985.
[13] Polonsky I, Keer L. A numerical method for solving rough contact problems based on the multi-level multi-summation and conjugate gradient techniques. Wear. 1999;231(2):206–219.
[14] Vollebregt E. A new solver for the elastic normal contact problem using conjugate gradients, deflation, and an FFT-based preconditioner. J Comput Phys. 2014;257:333–351.
[15] Kalker JJ. A fast algorithm for the simplified theory of rolling contact. Veh Syst Dyn. 1982;11(1):1–13.
[16] Vermeulen PJ, Johnson KL. Contact of non-spherical elastic bodies transmitting tangential forces. J Appl Mech. 1964 06;31(2):338–340.
[17] Shen ZY, Hedrick JK, Elkins JA. A comparison of alternative creep force models for rail vehicle dynamic analysis. Veh Syst Dyn. 1983;12(1–3):79–83.
[18] Kalker JJ. Book of tables for the Hertzian creep-force law. Delft (The Netherlands): Delft University of Technology; 1996.
[19] Polach O. A fast wheel–rail forces calculation computer code. Veh Syst Dyn. 1999;33:728–739.
[20] Sichani MS, Enblom R, Berg M. An alternative to FASTSIM for tangential solution of the wheel–rail contact. Veh Syst Dyn. 2016;54(6):748–764.
[21] Piotrowski J, Liu B, Bruni S. The Kalker book of tables for non-Hertzian contact of wheel and rail. Veh Syst Dyn. 2017;55(6):875–901.
[22] Ayasse JB, Chollet H. Determination of the wheel rail contact patch in semi-Hertzian conditions. Veh Syst Dyn. 2005;43(3):161–172.
[23] Sichani MS, Enblom R, Berg M. Wheel–rail contact modeling for damage predictions in dynamics simulation software. In: International Conference on Contact Mechanics of Wheel/Rail Systems, 08; 2015.

[24] Linder C. Verschleiss von eisenbahnrädern mit unrundheiten [dissertation]. Zürich: ETH Zurich; 1997. Nr. 12342.
[25] Piotrowski J, Kik W. A simplified model of wheel/rail contact mechanics for non-Hertzian problems and its application in rail vehicle dynamic simulations. Veh Syst Dyn. 2008 02;46:27–48.
[26] Liu B, Bruni S, Vollebregt E. A non-Hertzian method for solving wheel–rail normal contact problem taking into account the effect of yaw. Veh Syst Dyn. 2016;54(9):1226–1246.
[27] Sichani MS, Enblom R, Berg M. Comparison of non-elliptic contact models: towards fast and accurate modelling of wheel–rail contact. Wear. 2014;314:111–117.
[28] Pascal JP, Sauvage G. The available methods to calculate the wheel/rail forces in non Hertzian contact patches and rail damaging. Veh Syst Dyn. 1993;22(3–4):263–275.
[29] Ayasse JB, Chollet H, Maupu JL. Paramètres caractèristiques du contact roue-rail. INRETS Report Nr. 225; 2000.
[30] Pascal JP, Soua B. Solving conformal contacts using multi-Hertzian techniques. Veh Syst Dyn. 2016;54(6):784–813.
[31] Sichani MS, Enblom R, Berg M. A novel method to model wheel–rail normal contact in vehicle dynamics simulation. Veh Syst Dyn. 2014;52(12):1752–1764.
[32] Boussinesq J. Application des potentiels à l'étude de l'équilibre et du mouvement des solides élastiques. Paris: Gauthier-Villars; 1885.
[33] Cesbron J, Yin H, Anfosso-Lédée F, et al. Numerical and experimental study of multi-contact on an elastic half-space. Inter J Mech Sci. 2009;51(1):33–40.
[34] Reusner H. Druckflächenbelastung und oberflächenverschiebung im wälzkontakt von rotationskörpern [dissertation]. Germany: University of Karlsruhe; 1977.
[35] Love AEH. The stress produced in a semi-infinite solid by pressure on part of the boundary. Philos Trans R Soc London Sr A, Pap Math Phys Character. 1929;228(659–669):377–420.
[36] Ayasse JB, Chollet H, Sebès M. Wheel–Rail contact. In: Iwnicki S, Spiryagin M, Cole C, et al., editors. Handbook of railway vehicle dynamics. 2nd ed. Boca Raton: CRC Press/Taylor & Francis Group; 2019. p. 241–280. Chapter 7.
[37] Quost X, Sebès M, Eddhahak A, et al. Assessment of a semi-Hertzian method for determination of wheel–rail contact patch. Veh Syst Dyn. 2006;44(10):789–814.

Appendices

Appendix 1. Solving the contact problem for the normal force

The normal force acting on each strip N_i can be evaluated using Equation (15):

$$N_i = \pi \tilde{a}_i b_i p_{0_i}. \tag{A1}$$

The system of equations in matrix form is

$$\mathbf{u} = \mathbf{C}'\mathbf{N}, \tag{A2}$$

where $\mathbf{N} = \{N_1, \ldots, N_n\}^{\mathrm{T}}$, and the matrix of influence coefficients $\mathbf{C}'$ is given by

$$\mathbf{C}' = \begin{bmatrix} (\pi \tilde{a}_1 b_1) C_{11} & \ldots & (\pi \tilde{a}_n b_n) C_{1n} \\ \vdots & \ddots & \vdots \\ (\pi \tilde{a}_1 b_1) C_{n1} & \ldots & (\pi \tilde{a}_n b_n) C_{nn} \end{bmatrix}. \tag{A3}$$

The half-length of the contact patch at the end of each iteration can be computed using

$$\tilde{a}_i = \left(\frac{1}{2E^\star} \frac{n_i m_i^2}{A_i + B_i} \frac{1}{b_i} N_i \right)^{\frac{1}{2}}. \tag{A4}$$

Equations (A2) and (A4) can subsequently be employed in the algorithm presented in Figure 3 to solve the contact problem.

Appendix 2. Contact patch half-length using ANALYN

The expression for the contact patch boundaries in ANALYN [31] is

$$\tilde{a}_i = \sqrt{\frac{d_i}{[1+\alpha_i]A_i}}, \tag{A5}$$

where

$$d_i = \delta - [1+\beta_i]h_i. \tag{A6}$$

Here, d_i is the penetration and the term $\beta_i h_i$ takes the surface deformation into account analytically, as opposed to VP methods where the deformation is neglected. The coefficients α_i and β_i are defined as:

$$\alpha_i = \frac{r_i}{m_i^2}\left(1+\frac{B_i}{A_i}\right) - 1, \tag{A7}$$

$$\beta_i = \frac{r_i}{n_i^2}\left(1+\frac{A_i}{B_i}\right) - 1, \tag{A8}$$

where A_i and B_i are the relative longitudinal and lateral curvatures, respectively, while m_i, n_i, and r_i are non-dimensional Hertzian coefficients calculated using the local curvatures. The maximum pressure value p_{0_i} is

$$p_{0_i} = \frac{2E^*}{\pi}\frac{1}{n_i r_i}\frac{d_i}{\tilde{a}_i}. \tag{A9}$$

Squaring Equation (A5) and taking into account the expression for α_i, we have

$$d_i = \frac{r_i}{m_i^2}[A_i + B_i]\tilde{a}_i^2. \tag{A10}$$

Combining Equations (A9) and (A10), the half-length of the contact patch $\tilde{a}_i$ can finally be written as

$$\tilde{a}_i = \frac{\pi}{2E^*}\frac{m_i^2 n_i}{A_i + B_i}p_{0_i}. \tag{A11}$$